Static and Dynamic Propagation-Channel Impairments in Reverberation Chambers

Kate A. Remley, *Senior Member, IEEE*, Sander J. Floris, Haider A. Shah, and Christopher L. Holloway, *Fellow, IEEE*

***Abstract*—We study the separate and combined effects of static and dynamic multipath channels created in a reverberation chamber on bit-error-rate (BER) measurements of digitally modulated signals. We demonstrate measurement methods to identify individually sources of bit errors arising from a frequency selective channel and discuss why the speed of the mode-stirring paddle impacts the level of BER for certain modulated-signal data rates and bandwidths. An unloaded, high-*Q* reverberation chamber is studied in the 700 MHz frequency band to clearly illustrate both static and dynamic multipath effects. We describe a rigorous method for calculating the 95% confidence intervals of the measured BER and study the repeatability of the mode-stirring paddle. Our paper illustrates the importance of understanding the correct error bounds when identifying different sources of impairment.**

***Index Terms*—Bit error rate (BER), coherence bandwidth, digitally modulated signal, measurement, multipath, propagation channel, reverberation chamber, wireless system.**

I. Introduction

UNDERSTANDING channel impairments that may be introduced into the propagation environment by the reverberation chamber is essential when using these chambers for test and measurement of wireless devices that transmit digitally modulated signals. In this paper, we illustrate measurement methods for isolating and evaluating mechanisms that impair propagation channels in a reverberation chamber by direct measurement of digitally modulated signals.

The use of a reverberation chamber as a reliable, repeatable, and controllable environment for testing wireless systems has become increasingly popular. Applications have been recently developed that use reverberation chambers to emulate multipath propagation environments for free-field test of wireless devices. These include the implementation of Rayleigh and "hyper-Rayleigh" multipath environments [1]–[3]; measuring receiver sensitivity, total isotropic sensitivity (TIS), and other over-the-air test parameters [4]–[6]; measurement of *K*-factor (the ratio of direct-path to reflected received signal level) [7]; measurements of high-data-rate multiple-input-multiple-output (MIMO) techniques [8]–[10]; simulating the reverberant effects of various structures [11], [12]; measurements of bit error rate (BER) in static environments [13]; development of improved channel models [14]; and simulating environments with several clustered delay paths [15].

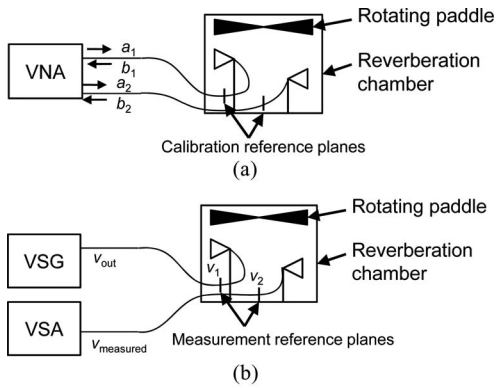

Fig. 1. Schematic overview of the reverberation chamber and measurement setups. (a) Incident and reflected traveling waves at the antenna ports were measured by the VNA. The wave variable a_i represents the voltage traveling wave incident on the antenna from VNA port i, and b_i represents the voltage traveling wave reflected back to VNA port i, due to reflections from the antenna or chamber (the second antenna is not driven). (b) Voltage measured at the input of the VSA was referred back to the same reference plane used in the VNA measurements.

Much of this prior work has focused on characterization of the reverberation chamber using a vector network analyzer (VNA) to conduct frequency-domain measurements (for example, [1]–[4], [7]–[10], and [12]) or on application-specific uses of the reverberation chamber, where specialized receivers, such as base-station emulators were used (for example, [5] and [6]). Here, we illustrate measurement methods that utilize digitally modulated signals to directly assess the impact of the multiple causes of bit errors. We use laboratory-grade, real-time instrumentation, including a vector signal generator (VSG) and vector signal analyzer (VSA) [16], to measure signals having no error correction or encoding.

As depicted in Fig. 1, a moveable mode-stirring paddle together with two antennas implement a time-varying multipath propagation channel within the reverberation chamber. When the paddle is stepped, a series of static, discrete-time, time-invariant channels [17] are established. Conversely, when the paddle moves continuously, a dynamic time-varying propagation channel is created within the reverberation chamber. When a digitally modulated signal is transmitted within the chamber,

Manuscript received March 11, 2010; revised September 3, 2010; accepted November 15, 2010. Date of publication April 7, 2011; date of current version August 18, 2011.

K. A. Remley, H. A. Shah, and C. L. Holloway are with the National Institute of Standards and Technology, Boulder, CO 80305 USA (e-mail: remley@boulder.nist.gov; hyder.a.shah@gmail.com; holloway@boulder.nist.gov).

S. J. Floris is with the National Institute of Standards and Technology, Boulder, CO 80305 USA, and also with the Faculty of Electrical Engineering, Eindhoven University of Technology, 5600 MB Eindhoven, The Netherlands (e-mail: s.j.floris@student.tue.nl).

Color versions of one or more of the figures in this paper are available online at http://ieeexplore.ieee.org.

Digital Object Identifier 10.1109/TEMC.2010.2100823

bit errors may be introduced by various propagation-channel impairments, including Gaussian receiver noise, the coherence bandwidth of the reverberation chamber, which is essentially a resonant cavity [18], as well as dynamic fading introduced when the paddles move.

The propagation channel created in a multipath environment, such as the reverberation chamber is said to be *frequency flat* when the frequency-domain response of static multipath reflections is independent of frequency within the modulation bandwidth of a signal. In the absence of other impairments, signals will be demodulated correctly if they are received with a sufficient signal-to-noise ratio (SNR). Otherwise, when static multipath reflections interfere constructively and destructively within the bandwidth of the modulated signal, the channel is considered *frequency selective*. In real-world wireless systems, a frequency selective channel can often be compensated in the receiver by use of an equalizer.

In the dynamic case, where the channel changes continuously due to, for example, paddle movement, the constructive and destructive multipath interference may create *fading*. For the case of *fast fading*, the duration of the fade is short enough that it impacts only a few symbols. Error correction can often compensate and the symbols will still be decoded correctly. For the case of *slow fading*, a deep fade may cause the channel to change continuously over a significant fraction of a frame, and the BER may increase. Finally, when fades occur more slowly than the frame duration, the receiver may interpret this as a simple change in received power level, and again may be able to compensate. See [17] for additional information on fading in wireless channels.

The speed at which the time-varying channel appears to be invariant to the receiver is given by the *coherence time*, a metric that is related to *Doppler spread.* As discussed in Section V, the coherence time in a high-Q reverberation chamber may change locally as a function of paddle position, causing intermittent fast fades even though the paddle velocity should provide a slow-fading channel. This effect has been discussed in prior work [19] and was observed in our measurements. Note that it is necessary to define the channel characteristics described earlier with respect to the modulation bandwidth and/or data rate of the signal.

In this paper, to readily identify physical impairments to the channel, we utilize simple digitally modulated signals of various bandwidths and data rates in a high-Q reverberation chamber. These signals are generated without the benefit of sophisticated error correction and equalization techniques, and without use of transmission schemes, such as orthogonal frequency-division multiplexing (OFDM) or code-division multiple access (CDMA), which are designed to compensate for multipath and fading. These techniques would be found in real-world wireless transmissions. However, to study the propagation channel directly, it is our goal to study—not suppress—bit errors. We implement only a simple error-correction algorithm to resynchronize our receiver after it loses lock due to a long, deep fade.

We demonstrate measurement methods that can be used to quantify both static and dynamic reverberation-chamber channel effects on wireless device performance. Specifically, we study channel impairments arising from 1) weak-signal (noisy) reception; 2) coherence bandwidth limitations; and 3) dynamic-channel fading. As we will show, the user can identify weak-signal effects and the impact of a channel's coherence bandwidth by means of stepped-paddle, static-channel measurements. Once these effects have been quantified, the user can then study the additional influence of dynamic-channel fading on BER.

II. Measurement Procedure

The unloaded reverberation chamber used in our tests is 2.8 m $\times$ 3.1 m $\times$ 4.6 m in size and is located at the National Institute of Standards and Technology (NIST), Boulder, CO. We used an unloaded chamber in order to clearly illustrate the concepts discussed in this paper. The high Q associated with the unloaded chamber accentuates the modulation-bandwidth-dependent effects of the multipath channel. These phenomena exist in lower Q chambers as well, but are more pronounced in a high-Q environment such as the one used here.

A. VNA Measurements

We measured chamber characteristics with a VNA and, separately, the effects of chamber-induced channel impairments on digitally modulated signals with a VSA. In both cases, the instruments were connected through a bulkhead connector to two dual-ridge horn antennas, as shown in Fig. 1. The antennas we used have an operating range from 200 MHz to 2 GHz and dimensions of 0.93 m $\times$ 0.98 m $\times$ 0.73 m. The antennas were pointed away from each other and toward the wall to minimize direct-path propagation. The same antennas were used for both VNA and VSA measurements.

For the VNA measurements, depicted in Fig. 1(a), the VNA was calibrated at the reference planes indicated in Fig. 1 before the antennas were connected. We acquired VNA measurements of the channel response by stepping the large, single paddle, and letting it settle before each measurement. We stepped the frequency over a 100 MHz bandwidth around a center frequency of 700 MHz in each measurement, with 16 001 points used for a frequency resolution of 6.25 kHz. The rms delay spread averaged over all measurements was approximately 700 ns [13].

The antennas and cables used were quite well impedance matched over our frequency band of interest. As such, we neglected reflections from the input port of the antenna to the second port of the VNA (i.e., we assumed $S_{22}(f) = 0$). In this case, the frequency-dependent complex transfer function $H(f, \theta_i)$ for each paddle position θ_i is given by

$$H(f,\theta)|_{\theta_i} = S_{21}(f) \tag{1}$$

where $S_{21}(f)$ is the complex transmission parameter.

B. BER Measurements

As illustrated in Fig. 1, by replacing the VNA with the VSA, it is possible to create a one-way communication system having the same multipath channel as that described earlier. We used

the method of [16], briefly summarized here for clarity. We generated a binary-phase-shift-keyed (BPSK) signal of binary digits (bits) by use of the VSG. A pseudorandom sequence of 2048 BPSK-modulated bits was transmitted repeatedly into the chamber. The VSA was then used to demodulate the 2048-bit received frames from the chamber with a coherent detector as well as to measure the received power, frequency averaged across the signal's bandwidth, and time averaged across each frame. The transmitted power was swept in order to separate bit errors caused by random noise from those caused by other sources. The BER was calculated as the ratio of erroneously received bits to the total number of received bits.

The method discussed in [16] describes the use of a cross correlation of the received bits with the known, generated bits to correct for the time-variant path delay created by the rotating paddle. It also describes a rudimentary method that we implemented to compensate for the loss of receiver synchronization when the receiver encountered a deep fade during a frame. This method, implemented in postprocessing, monitors the BER level for each received frame. When 32 bits or more are received with a BER of 1 (not 0.5 as would be expected in the worst case for our BPSK signal), we assume receiver lock has been lost and the symbols are redefined. The erroneous 32 bits are considered to represent "burst errors" and are filtered out. Using this technique, we avoid including long streams of bit errors in our BER calculation that were caused by loss of receiver synchronization, rather than by the instantaneous channel conditions.

The frame of 2048 pseudorandom bits that we used was generated by the Marsenne Twister algorithm [20]. This algorithm is designed to achieve a statistically uncorrelated sequence that has a white-noise-like autocorrelation. We chose this algorithm because it is a robust technique that is independent of the length of the bit sequence, unlike some of the built-in functions in numerical packages that we tested. To minimize intersymbol interference, the frame length was chosen such that, for all of our chamber channel impulse response measurements, the power of the first bit in the frame had decayed significantly before the next frame was transmitted. This ensured that little correlation occurred between successive frames in the multipath environment, so that the pseudorandom nature of the signal remained essentially unchanged.

For a BPSK-modulated signal, the null-to-null bandwidth is approximately equal to [17]

$$B \approx (1+\alpha) R_{\text{symbol}}, \tag{2}$$

where α is the root-raised cosine filter roll-off factor, which was set to 0.35, the value used in many transmission standards for digitally modulated signals. We measured the BER for BPSK-modulated signals having three different data rates: 24.3 ks/s (having a null-to-null bandwidth B of approximately 32.8 kHz), 243 ks/s (with B of $\sim$328 kHz), and 768 ks/s (with B of $\sim$1.037 MHz).

To compare the BER from these signals, we reduced the angular step of the paddle for higher symbol rates. As the symbol rate increases, the transmission time of a frame decreases and, for a continuously turning paddle, the paddle displacement during the measurement of a frame decreases. Because we wished to measure BER over every frame that would be transmitted by a continuously turning paddle, we carried out measurements for finer and finer paddle angles for higher data rates. The paddle-angle increments at which measurements were made are illustrated in Table I. Also shown in Table I are the number of measured power levels and the number of bits recorded at each power level.

TABLE I
MEASUREMENT PARAMETERS FOR OUR STUDY OF THE EFFECTS OF STATIC AND DYNAMIC CHANNEL IMPAIRMENTS ON DIGITALLY MODULATED SIGNALS

Symbol rate/frame duration (2048 bits)	Paddle movement (r/min)	Traversed angle, θ_{paddle}	# of meas. in a full paddle rotation, M	# power levels	# of bits meas. for each power level (Mb)
24.3 ksps/ 84.25 ms	stepped	0.5°	720	96	1.47
	1	0.51°	712	96	1.54/ 3.20
	2	1.01°	356	8	1.47
	4	2.02°	178	8	1.47
	6	3.03°	119	-	-
243 ksps/ 8.43 ms	stepped	0.05 °	7200	8	14.7
	1	0.05°	7115	9	14.75
	2	0.10°	3561	17	7.37
	4	0.20°	1780	80	3.69
	6	0.30°	1187	80	2.45
768 ksps/ 2.70 ms	stepped	0.01 °	36000	13	8.87/ 43.22
	1	0.016°	22500	33	17.88
	2	0.032°	11250	-	-
	4	0.064°	5625	18	12.29
	6	0.096°	3750	18	8.19

For a continuously moving paddle [where angular velocity is represented in revolutions per minute (r/min)], the traversed angle is a calculated quantity. When various numbers of bits were acquired over multiple power levels, the minimum/average number of bits is shown. Entries are missing for cases that were not measured.

As will be shown in Section IV, it was not necessary to measure a large number of power levels for the higher data rate signals because the BER was very high due to the limited coherence bandwidth of the chamber. Because the reverberation chamber creates a distribution of received power levels for every transmitted power level (see [16], for an example), we easily obtained a minimum of 1000 bit errors for every received power level, as desired for a statistically significant measure of BER. The choice of the number of measured bits is discussed in more detail in the uncertainty section of this paper.

After measuring the BER at the specified number of paddle positions, we grouped the results with respect to the measured received power in 1 dB steps. The measured BER values at each received power were averaged. In the following sections, BER is plotted with respect to a normalized SNR, E_b/N_0, where E_b is the energy per bit (defined as the average power in an infinitely long message divided by the symbol rate) and N_0 is the spectral noise density [17]. This metric is determined by means of (2) with

$$\frac{E_b}{N_0} = \frac{S}{N}\frac{B}{R_{\text{symbol}}} \approx (1+\alpha)\frac{S}{N}, \tag{3}$$

where S is the received power averaged across the modulation bandwidth, and N is the frequency-averaged noise power within the signal band. N was found by connecting a 50-Ω load to our VSA and recording the measured power in the band.

The measurement setups and set of excitation signals described earlier allowed us to identify and quantify the effects on BER of weak-signal reception, channel coherence bandwidth, and fading. These methods are discussed individually in the following sections.

III. Channel Impairments Due to Weak-Signal Reception

Additive white Gaussian noise (AWGN) will be introduced into the measurement of a signal via receiver noise in reverberation chamber measurements, and this impairment will become appreciable when the received-signal level is close to the noise floor of the receiver. Such weak-signal reception also occurs in a free-space AWGN propagation channel consisting of a line-of-sight path and no fading. When the signal-to-noise level is low enough, a receiver without error correction will report a BER of 50% for a BPSK-modulated signal, because there is an equal chance that the bit will be estimated as either of the two possible symbol values. To measure this effect, it is only necessary to excite the reverberation chamber with a signal having a low enough SNR that the BER is 50%. This will be illustrated graphically later in the paper (see Figs. 4, 10, and 11).

Because the effects of the receiver noise are additive, this weak-signal effect may be measured in either a static or a dynamic channel. As the input power increases, effects related to other types of channel impairment become apparent, as described in the following sections.

IV. Impairments Due to Limited Coherence Bandwidth

A. Autocorrelation Function and Coherence Bandwidth

The average bandwidth over which frequency components of a signal in a given propagation environment have strong correlation is a statistical measure called the *coherence bandwidth*. When the bandwidth of a transmitted signal exceeds the coherence bandwidth of a channel, the channel will induce frequency-selective distortion in the received signal. Uncorrected, this distortion may cause bit errors. Because of this frequency-selective behavior, bit errors occur independent of signal strength and give rise to BER values that are irreducible without the application of error correction techniques. As discussed in the following, these effects may be identified using stepped-paddle measurements.

Coherence bandwidth is usually defined from the frequency autocorrelation function obtained by averaging multiple measurements of a multipath channel. It is generally assumed that the channel does not change significantly over the course of an individual measurement. A common method for finding the complex autocorrelation function by use of the transfer function is described in [17]

$$R(\Delta f, \theta_i) = \int_{-\infty}^{\infty} H(f, \theta_i) H^*(f + \Delta f, \theta_i) \mathrm{d}f, \qquad (4)$$

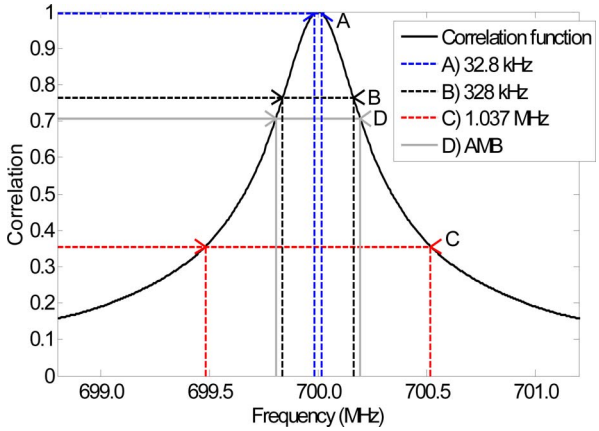

Fig. 2. Occupied bandwidth, defined in (2), for 24.3, 243, and 768 ks/s BPSK signals (dashed lines) superimposed on the correlation function. The correlation function (solid line) was calculated from measurements made at 360 paddle positions in an unloaded, high-Q reverberation chamber. The average mode bandwidth (AMB) indicated by D is 387.4 kHz.

where $H(f)$ is a continuous function, θ_i is the ith paddle angle (out of M), Δf defines the bandwidth of interest, and the asterisk denotes complex conjugation. Each paddle position θ_i corresponds to a measurement of the ith channel in the propagation environment, similar to measurements made in time-varying multipath environments at different times and/or locations. In the following coherence bandwidth calculations, we assume independence between our individual channel measurements because of the extremely high Q of our chamber.

The M autocorrelation functions from (4) are averaged over all stirrer positions at each frequency point (giving the expectation of the channel), and then, a threshold value is chosen above which the channel is said to be coherent. Typical values of 0.9, 0.7, $1/e$, or 0.5 are used [21]–[24]. Understanding how this threshold is chosen is of importance for those studying the effects of frequency selectivity on digitally modulated signals.

To characterize the coherence bandwidth in the reverberation chamber, we use a VNA to measure multiple channel transfer functions created by different fixed paddle positions in the reverberation chamber. Because the VNA measures a discrete set of frequencies, the discrete autocorrelation function is used, with an appropriate discretization of f and $f + \Delta f$, respectively.

The expectation, normalized to a maximum value of 1, measured in the unloaded NIST reverberation chamber for a carrier frequency of 700 MHz is shown in Fig. 2 for 360 channel measurements (360 different paddle angles θ_i). The bandwidths of the three BPSK signals are also marked in this figure, to link the modulation bandwidth and BER to the correlation function. The average mode bandwidth (AMB, the 3 dB bandwidth of a mode) [24] is defined for a correlation threshold value of $1/\sqrt{2}$ and is indicated by "D" in Fig. 2.

We confirmed that our unloaded reverberation chamber excites uncorrelated scattering by observing the symmetry of the frequency correlation function in Fig. 2 [22]. This means that the channel is time invariant for each stepped-paddle position.

The variation in the autocorrelation function calculated for three different bandwidths [i.e., for three different values of

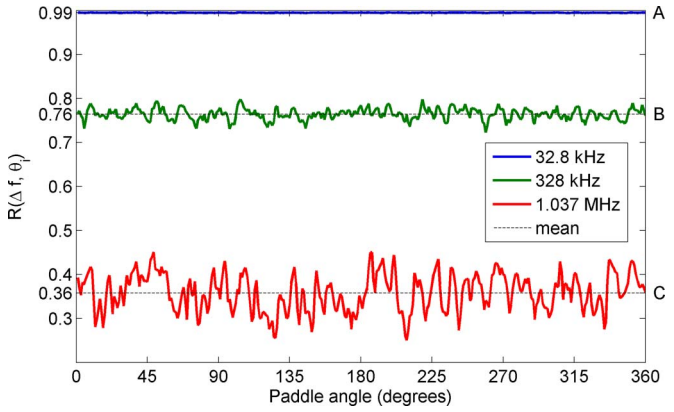

Fig. 3. Variation of the autocorrelation function (4) for three different signal bandwidths Δf as a function of stepped paddle position θ_i measured every 1°. The standard deviation for each of these products is A) 3.0e-4, B) 0.013, and C) 0.042.

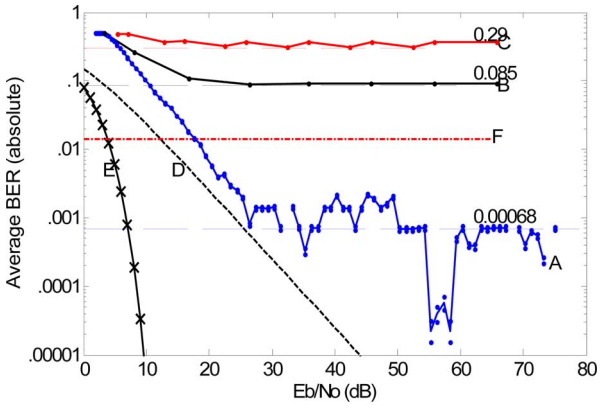

Fig. 4. BER as a function of E_b/N_0 for stepped-paddle measurements. The BPSK-modulated signals have data rates of A) 24.3 ks/s, B) 243 ks/s, and C) 768 ks/s. Curve D represents the BER for an ideal Rayleigh-distributed (fading) channel and curve E represents an ideal AWGN channel. Curve F denotes 1.4% BER. The BER is averaged over all paddle positions. The 95% confidence bounds are shown by dots around the data.

Δf in (4)] is shown in Fig. 3 as a function of paddle position. We compute the autocorrelation for a single VNA measurement at each paddle position. Fig. 3 shows that a larger variance in the predicted coherence bandwidth can be expected for lower threshold values, affecting wider bandwidth signals more than narrowband signals, as quantified by the standard deviation given in the caption of Fig. 3.

B. BER Measurement and Static Impairments

1) Measuring BER: Fig. 4 shows the measured BER for the "A" 24.3 ks/s, "B" 243 ks/s, and "C" 768 ks/s signals. For comparison, the BER for an ideal Rayleigh channel is indicated with "D" and that of an ideal AWGN channel is indicated with "E" in Fig. 4. The latter can be found from the well-known formula $P_e = Q(\sqrt{(2E_b/N_0)})$ [17], where P_e is the probability of a bit error for a BPSK-modulated signal.

At the lowest values of E_b/N_0, Fig. 4 shows that all three signals have a BER of 0.5, corresponding to an ideal AWGN channel, where the likelihood of receiving a correct bit is the same as that of receiving an incorrect bit. As the E_b/N_0 increases, the BER decreases. However, for E_b/N_0 levels well above the noise floor of the receiver, an irreducible (when uncorrected) BER level is observed, indicating that mechanisms other than the value of received power are responsible for causing the bit errors. Fig. 4 also clearly shows an increase in the BER as the occupied bandwidth of the signal is increased.

Note that the high levels of BER in curves B and C do not preclude the use of the reverberation chamber for wireless test. As discussed earlier, in this paper, we have intentionally used a high-Q chamber with no sophisticated error correction to illustrate the physical sources of bit errors and impairment identification methods.

2) Uncertainty in the Measured BER: We define the measured BER as the ratio of the erroneously received bits to the total number of received bits in a data stream. The actual BER is defined by the BER we would measure if the sample were infinitely large. However, we can estimate the interval that contains the actual BER with 95% confidence from our measurement made with a limited number of samples.

If we consider the received set of bits as a random variable, BER corresponds to the variance around the correct set of transmitted bits, typically given in percent. As such, the variation in the measured BER in a series of measurements is essentially the variance of a variance, rather than simply the variance of a measured physical quantity (such as an analog voltage). As a result, to find the 95% confidence interval for the actual BER, we used techniques to find the 95% confidence interval of a variance. Because the measured estimate of the BER takes on discrete values that, if purely random, may be described by the binomial distribution, the confidence interval for the actual BER is estimated from the inverse of the cumulative distribution of the Beta function, rather than the cumulative chi-squared distribution, as would be the case for a series of analog voltage measurements. This is also discussed in the context of BER simulation in [25].

The cumulative distribution of the Beta function can be found in many software packages. For example, the software package that we used took the following variables as inputs to the inverse of the Beta cumulative distribution function: 1) the lower/upper edge of the 95% confidence bound (0.025 and 0.975, respectively); 2) the number of bit errors; and 3) the total number of measured bits minus the number of bit errors.

Our estimated 95% confidence intervals, shown by dots in Fig. 4, are quite small, indicating that we obtained enough samples to estimate the actual BER at each received power level.

3) Interpretation of BER Curves in Reverberation Chamber Measurements: Fig. 4 shows that the received signal power relative to the noise power in the receiver essentially determines BER for the lower values of received power. As the received power increases, the BER decreases until the received signal is well above the noise floor of the receiver, at which point an irreducible level of BER is observed, not correlated with received power. This level of BER is irreducible when error correction is not used.

Above the noise floor of the receiver, a comparison of Figs. 2 and 4 shows that the uncorrected irreducible BER appears to be well correlated to the limited coherence bandwidth of the channel for wider bandwidth signals. That is, the irreducible

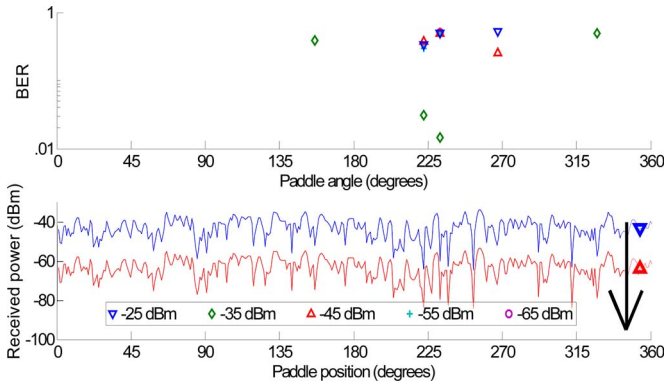

Fig. 5. Measurements of BER (top graph) and received power averaged over a 32.8 kHz bandwidth (bottom graph) as a function of stepped paddle position, measured every 1° for a 24.3 ks/s BPSK-modulated signal. For clarity, only two power levels are shown in the bottom graph. The symbols in the top graph correspond to five different transmitted power levels, shown by the legend in the lower graph. The absence of a symbol at a given paddle position indicates no bit errors were detected.

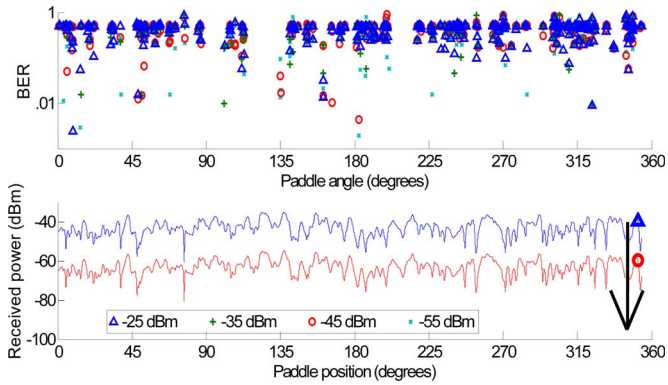

Fig. 6. Measurements of BER (top graph) and received power averaged over a 328 kHz bandwidth (bottom graph) as a function of stepped paddle position, measured every 0.05° for a 243 ks/s BPSK-modulated signal.

BER level is not a function of received power and is higher for signals with wider modulation bandwidths.

However, we would not expect to see such a high, variable level of irreducible BER for the 24.3 ks/s signal. Figs. 2 and 3 indicate the channel should be frequency flat for this narrowband signal. Because these variations greatly exceed our 95% confidence bounds, we know that the variation is not due to an insufficient number of data points in our measurement samples. This indicates that a mechanism not correlated to received power is inducing bit errors.

The top graph in Fig. 5 plots the BER for the 24.3 ks/s signal as a function of paddle position for five different transmitted power levels. The received frequency-averaged channel power is displayed in the lower graph of the figure for two of the transmitted power levels and the same paddle positions. We conducted these measurements for several different excitation power levels in order to separately identify the BER caused by power-dependent effects from those caused by other effects. In Fig. 5, the different symbols refer to different transmitted power levels, and the absence of a symbol at a given paddle position indicates no bit errors were detected.

Fig. 5 shows there is a good correlation between BER and paddle position, especially at two paddle positions near 225°, where we see bit errors occurring at nearly identical rates for at least four of the five excitation power levels. This indicates that the higher-than-expected, variable BER values shown in Fig. 4 for the 24.3 ks/s, signal are caused by a mechanism that is a function of paddle position rather than power. Such a mechanism could include a local change in the coherence time as a function of paddle position, or the fact that as the paddle turns, reflected signals may cause the receiver to experience a severe impedance mismatch. Such deep nulls have been noted to cause a "worse than Rayleigh" channel [26], [27]. Investigation of these effects on measured BER is the subject of current research at NIST.

Fig. 6 shows a plot of BER versus paddle position for the 243 ks/s signal. The bandwidth of the signal for this data rate nearly matches a coherence bandwidth having a threshold of 0.5, as shown in Fig. 2. We see a significant increase in the number of bit errors and the paddle positions where they occur. It is clear that the limited coherence bandwidth is the primary source of the uncorrected irreducible BER in this case.

To conclude our study of the static channel, we compare our measured performance to that predicted for an AWGN channel in [28]. We first find the ratio of our empty reverberation chamber's rms delay spread $\tau = 700$ ns to the symbol period T for the 24.3 ks/s BPSK signal. This ratio $\tau/T \approx 0.017$ yields a theoretically derived irreducible BER of approximately 1×10^{-4} (with no error correction) for an AWGN channel with a Gaussian power delay profile in [28]. As mentioned, the higher mean BER of 6.8×10^{-4} that we observe may be caused by high levels of impedance mismatch at certain paddle positions or the rapidly varying channel.

The present section has described methods to isolate and quantify impairments in the static channel. We showed that finding the 95% confidence bounds can help to differentiate the various effects that cause bit errors. As was demonstrated, because the uncorrected irreducible BER is independent of the signal strength, only signals well above the noise floor need to be measured to quantify the effects of the coherence bandwidth. As well, plotting BER as a function of paddle position can be used to isolate the variation in the irreducible BER in cases of low BER. While impairments of Gaussian noise and limited coherence bandwidth are present in dynamic channels as well, measuring these effects in a static channel allows the user to separately quantify these effects.

V. Dynamic-Channel Impairments

To study the effect of a dynamically changing channel on BER, we next implemented a continuously time-varying channel in the reverberation chamber. The single, large paddle was set to turn continuously, with a shaft velocity on the order of 1–6 r/min. Because the channel was time varying, for some data rates the receiver had to contend with signal levels and transfer functions that changed over the duration of the 2048-bit frame. The effects on BER may be quantified using the measurement methods described in the following.

A. Coherence Time and Doppler Shift

Just as the coherence bandwidth is a statistical measure of frequency selectivity of the channel, the coherence time is a statistical measure of time selectivity of the channel. It is the duration over which a dynamically changing channel can be assumed invariant with respect to the data rate of the signal [17], [22]. The coherence time is inversely proportional to Doppler shift in the frequency domain. Coherence time T_c is often given by $1/f_d$, with a more conservative value of $0.423/f_d$ sometimes used as well [17], where f_d is the maximum Doppler frequency. The Doppler frequency is calculated by

$$f_d = \frac{v}{\lambda} = \frac{vf}{c}, \tag{5}$$

where v is the relative speed between transmitter and receiver, f is the center frequency, and c is the speed of light. As long as the symbol time is much shorter than the coherence time, Doppler shift should not affect the BER.

We first consider the case where the Doppler shift is found solely from the velocity of the paddle. In our experiments, the paddle moved with a maximum velocity of 6 r/min. At this velocity, the paddle makes one full rotation in 10 s. The paddle has a radius of 1.2 m. Therefore, the tip of the paddle moves with a velocity of

$$v_{\text{paddletip}} = \frac{2\pi r}{T_{\text{rot}}} \approx 0.7 \text{ m/s}, \tag{6}$$

where r is the radius of the paddle and T_{rot} is the duration of a full rotation. This speed is equal to 2.7 km/h, which is close to the average speed of a walking pedestrian.

If we consider this speed to be the estimate of the relative speed between the transmitter and receiver, then a signal with a frequency f of 700 MHz would experience a Doppler shift of

$$f_d = \frac{v_{\text{paddletip}} f}{c} = 1.75 \text{ Hz}. \tag{7}$$

Theoretically, this would be the maximum Doppler shift for this environment. The value of Doppler shift in (7) corresponds to a coherence time of approximately $0.423/f_d = 242$ ms. For the coherence time to cause rapid enough channel changes to affect performance, the symbol rate would have to be lower than 4.1 s/s.

However, in a reverberation chamber, the same wave may hit the moving paddles several times after being reflected by chamber walls; therefore, the Doppler frequency may be larger for some paddle positions [19]. To illustrate this, in Fig. 7(a), we have plotted received power for a single-tone signal for 360 paddle positions. The top axis represents the time corresponding to the paddle continuously turning at 1 r/min. The time between dots corresponds to the duration of a single frame for each of the three different data rates. We see that the received power can change by as much as 30 dB during the transmission of one frame of the 24.3 ks/s signal. These rapid changes in power may have the effect of shortening the coherence time on a local timescale.

To quantify this, we calculated the coherence of the channel at paddle position θ_i with respect to stepped paddle positions

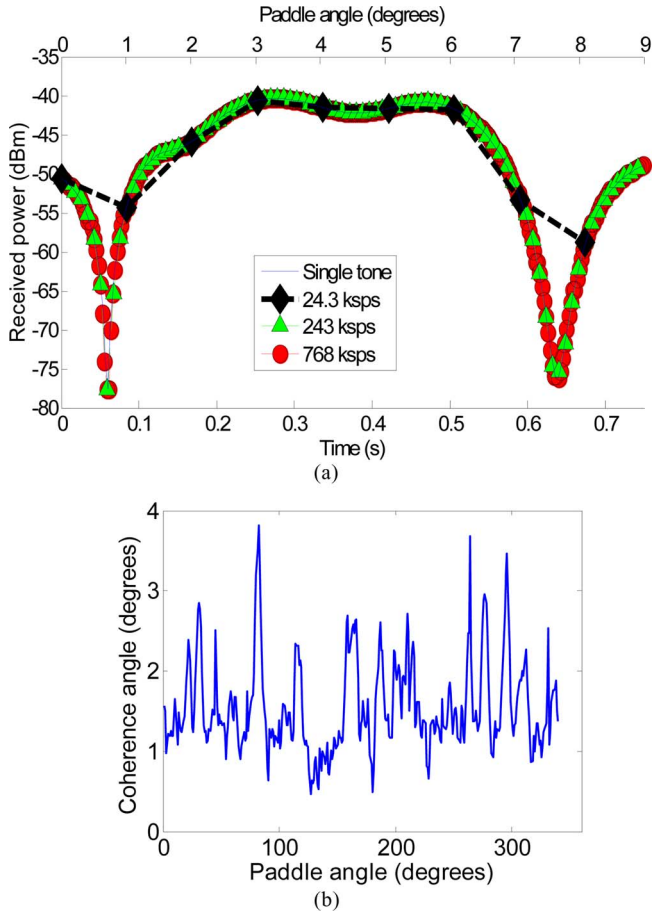

Fig. 7. (a) Frequency-averaged received power for a single tone at 700 MHz indicates the potential impact of a null in received power on signals having different data rates as the paddle turns. The duration of a single frame is indicated between two dots when the paddle rotates at 1 r/min. (b) Plot of the angular spread of paddle positions over which the channel is correlated, calculated with a threshold of 0.7.

within $\pm 10^\circ$ of θ_i. While coherence time would typically be calculated over all channel realizations (paddle positions), this "coherence angle" is proportional to the coherence time found over a localized set of channels. The coherence angle was found from the autocorrelation of the measured transfer function taken with respect to angle instead of frequency. The results are plotted in Fig. 7(b). From Fig. 7(b), the minimum value of coherence angle (coherence threshold of 0.7) is 0.46°. With a 1-r/min rotation speed at a frequency of 700 MHz, this corresponds to a localized coherence time of approximately 77 ms. Because our receiver's equalizer is set once per frame, we do not expect it to track a rapidly changing channel over a duration less than the frame rate of 84.25 ms for the 24.3 ks/s signal. Thus, we expect to see an increase in BER when the paddle is moving, compared to the static case. This effect will be higher for faster paddle speeds.

B. BER Measurements

In order to relate measured BER to the multipath created by the dynamically fading channel within the reverberation chamber, a continuous-time measurement of the modulated signal is

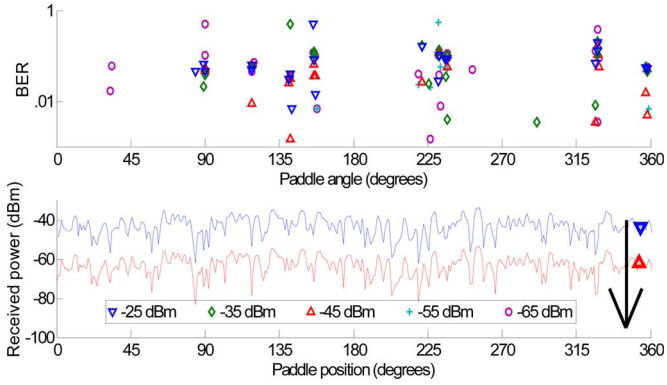

Fig. 8. Measurements of BER for five transmitted power levels (top graph) and received power averaged over a 32.8 kHz bandwidth (bottom graph) as a function of rotating paddle position, measured every 1° for a 24.3 ks/s BPSK-modulated signal. The paddle was continuously turning at 2 r/min. For clarity only two transmitted power levels are shown in the bottom graph.

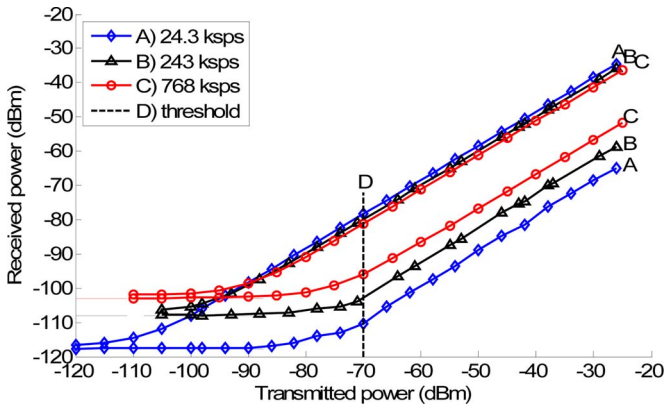

Fig. 9. Maximum (upper curves) and minimum (lower curves) received power over all paddle positions averaged over three different digitally modulated signal bandwidths at 1 r/min.

required. To do this, we acquired a continuous-time recording of the signal measured by the VSA. We then segmented the recording into 2048-bit frames in postprocessing. From the recorded RF waveforms, we calculated the received power, and from the demodulated signals, we calculated the BER.

In Fig. 5, we showed measurements of BER for a stepped paddle. In Fig. 8, we show measurements of BER with a paddle moving continuously at 2 r/min as a function of paddle position for the 24.3 ks/s BPSK signal. Again, the carrier frequency is 700 MHz.

In Fig. 5, very few bit errors were seen over the wide range of power levels and paddle positions. In Fig. 8, we see a significant increase in the number of bit errors. We see a strong correlation in bit errors to paddle positions where the channel presents a deep fade or a series of rapid fades to the transmitted signal.

Fig. 8 shows that the BER for the 24.3 ks/s signal takes on a range of values different from 0.5, indicating that our increase in BER in Fig. 6 is not due simply to the received signal level dropping below the noise floor of the VSA. We verify this in Fig. 9 by plotting the maximum and minimum in measured received power averaged over a specified bandwidth at all paddle positions as a function of transmit power. For transmit powers

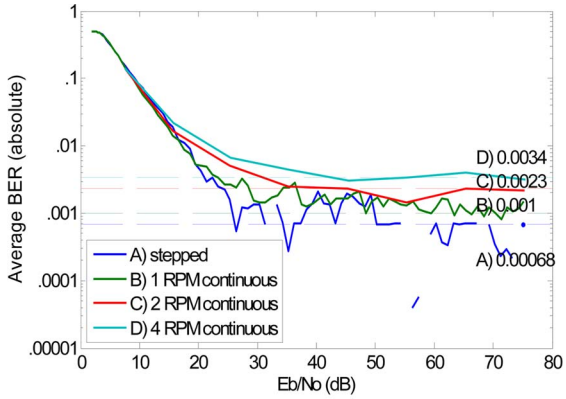

Fig. 10. BER averaged over a 360° paddle rotation for a 24.3 ks/s BPSK-modulated signal. The lowest BER is observed for the stepped paddle, and the BER increases as the paddle speed increases. The 95% confidence bounds are reported in Table II.

greater than –70 dBm, we see that the entire fade is captured above the noise floor threshold of the measurement system.

Fig. 10 shows the BER for the 24.3 ks/s as a function of E_b/N_0 averaged over 360 paddle positions. We again see that the primary cause of BER is Gaussian noise for low input signal levels, whether the channel is static or dynamic. As discussed earlier, the uncorrected irreducible BER for the static channel is approximately 0.00068. As predicted, the BER increases when a dynamic channel exists. This effect becomes more severe as the paddle speed increases, indicating that multiple fades during a given frame are degrading the performance of the receiver.

For signals with higher data rates and correspondingly wider modulation bandwidths, coherence bandwidth effects dominate both static and dynamic channels. Fig. 11(a) confirms this, showing that the uncorrected irreducible BER is not significantly affected by the paddle speed because the static channel effects dominate. Fig. 11(b) shows a similar effect for a 768 ks/s BPSK signal. Again, note that the extremely high values of BER are due to our intentional use of uncoded and uncorrected digitally modulated signals in a high-Q reverberation chamber for illustrative purposes.

We computed the average of the 95% confidence bounds for each of the curves shown in Figs. 10 and 11. These are reported in Table II. These statistics show the level to which we may have confidence in the differences and similarities in the curves, based on the number of bit error samples that we measured.

The results of this section show that received signal impairments caused by limited coherence bandwidth exist in both static and dynamic channels, and that they can overshadow impairments caused by fading for signals that exceed the coherence bandwidth. It is also clear that for flat-fading signals not exceeding the coherence bandwidth, the coherence time, which can be locally variable in the reverberation chamber, can impact BER. To study the effect of dynamic fading on modulated signals, continuous-time recording can be used effectively.

VI. Repeatability

In the previous sections, we have stated that the reverberation chamber can create a repeatable environment for free-field

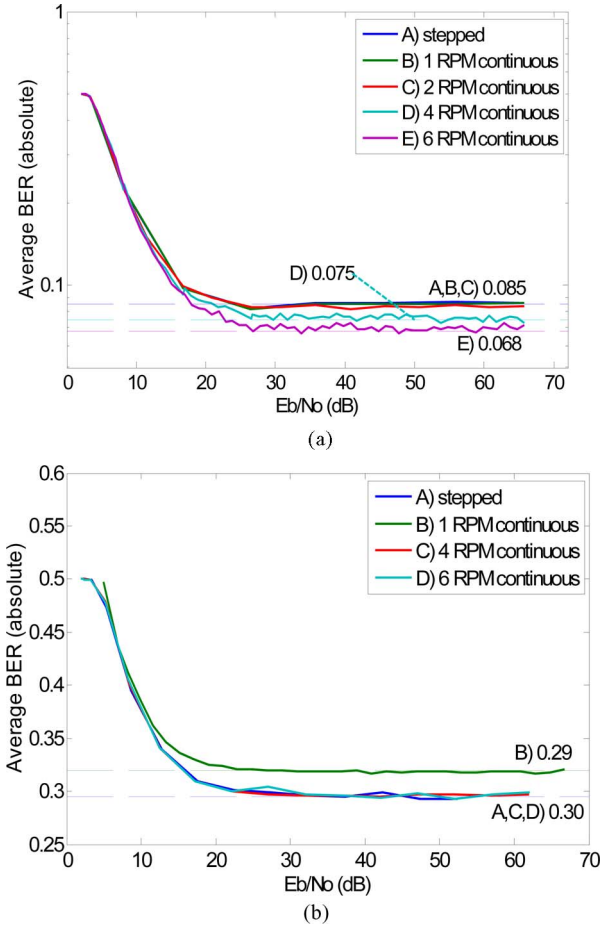

Fig. 11. BER averaged over a 360° paddle rotation for (a) 243 ks/s BPSK-modulated signal and (b) 768 ks/s BPSK signal. The uncorrected irreducible BER level for the 243 ks/s signal is approximately 8.5% and approximately 30% for the 768 ks/s signal. The 95% confidence bounds are reported in Table II.

TABLE II
AVERAGE 95% CONFIDENCE BOUNDS FOR THE DYNAMIC-CHANNEL BER MEASUREMENTS REPORTED IN FIGS. 10 AND 11

Paddle Speed	*24.3* ks/s	*243* ks/s	*768* ks/s
1 r/min	9.3 e-5	0.00029	0.00043
2 r/min	0.00027	0.00041	---
4 r/min	0.00030	0.00056	0.00052
6 r/min	---	---	0.00063

Average was taken over the irreducible BER portion of the curve.
Confidence bounds are reported in absolute units, with a maximum value of 1.

measurements. We have also seen the importance of measuring BER as a function of paddle position to quantify error mechanisms related to static and dynamic fading. To assess the repeatability of the measurement setup as a function of paddle position, we plot the variation in received power for repeat measurements. We utilize 0.5° stepped-paddle measurements of the 24.3 ks/s signal made at different transmit power levels. The received power was frequency averaged over the 32.8 kHz bandwidth of this signal for transmit power levels of −25, −35, −45, and −55 dBm. To compare signals transmitted at different power

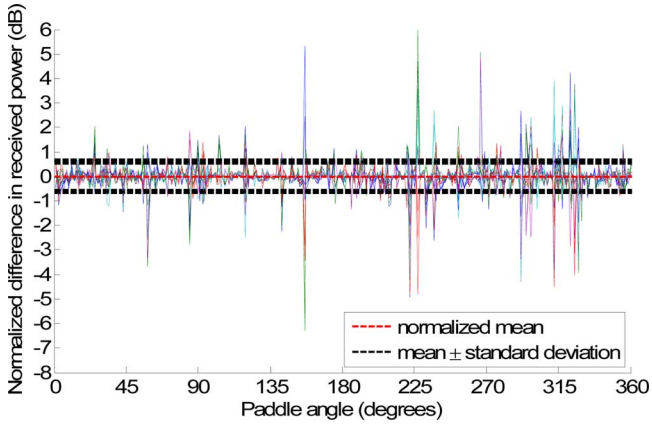

Fig. 12. The repeatability of the paddle, shown by the normalized difference (in decibels) between multiple received-power measurements (averaged over a 32.8 kHz bandwidth) as a function of paddle position. The standard deviation calculated over all paddle positions is also shown.

levels, we first found the difference (in decibels) between the received signals and then normalized the mean to zero decibel. Finally, we calculated the standard deviation of these differences, shown in Fig. 12. This variation was used to assess the repeatability of paddle position in our measurements. The calculated standard deviation was 0.6 dB. By referring to the original received-power graph in Fig. 5, we see that a rapid variation in received power causes the decibel difference to exceed the standard deviation.

VII. CONCLUSION

We presented measurement methods and associated uncertainty calculations to isolate and quantify the effects on BER of both static and dynamic channel impairments created in a reverberation chamber. Our paper focused on direct measurement of digitally modulated signals, with VNA measurements used to help identify mechanisms that introduced bit errors into the received signal.

We showed that weak-signal, Gaussian noise effects, and impairments due to limited coherence bandwidth can be measured with a stepped paddle. We illustrated that, for signal levels above the noise floor, a small coherence bandwidth may cause an irreducible BER level if no error correction is carried out, as expected. We found that, for narrowband signals, variations in the irreducible BER can be caused by paddle-position-dependent effects. The measurements presented in Section IV illustrated clearly that the definition of a "small" coherence bandwidth is relative to the occupied bandwidth of the digitally modulated signal being transmitted.

We also described measurement methods that can be used to study the increase in BER when dynamic fading is present. For these measurements, the paddle moved continuously and we illustrated a technique in which a continuous time recording was made of the digitally modulated signal. These measurements allowed us to readily determine that the dynamic sources of channel impairment more severely impacted the lower-data-rate signal. Measurements indicated that the cause was a locally

changing coherence time caused by a rapidly varying channel. Because of this, the uncorrected irreducible BER level for this low-data-rate signal increased with paddle speed. For wider bandwidth signals, the effects of increasing paddle speed were not as prominent because the bit errors introduced by the dynamic movement of the paddle were overshadowed by those introduced when the coherence bandwidth is narrow relative to the occupied bandwidth of the signal.

This paper showed that to isolate various channel-impairment effects, it is convenient to first characterize the weak-signal and coherence bandwidth with a stepped paddle. Once these effects are well characterized, the user may then isolate how dynamic fading affects the BER.

The work here is intended to provide the user with an understanding of the multiple impairments that a reverberation chamber may impart on a wireless communication signal, and to provide measurement techniques that isolate and quantify them, including measurement uncertainties and their respective confidence bounds. Even though our study focused on BPSK-modulated signals, similar results can be expected for other types of signals, including those that utilize amplitude modulation. After identifying the various sources of bit errors in a given reverberation chamber environment, the wireless engineer can then create an appropriate test environment for a specific application.

ACKNOWLEDGMENT

The authors would like to thank J. Ladbury and G. Koepke of NIST for their advice and technical support in this study, and D. Williams and C. M. Wang of NIST for advice on deriving the 95% confidence bounds on the measured BER. They would also like to thank A. G. Tijhuis of the Eindhoven University of Technology and D. W. Matolak of Ohio University for their advice and support. Finally, they would like to express their appreciation to the anonymous reviewers for their insightful comments.

REFERENCES

[1] M. Otterskog and K. Madsen, "On creating a nonisotropic propagation environment inside a scattered field chamber," *Microw. Opt. Technol. Lett.*, vol. 43, no. 3, pp. 192–195, Nov. 2004.

[2] C. Orlenius, M. Franzén, P.-S. Kildal, and U. Carlberg, "Investigation of heavily loaded reverberation chamber for testing of wideband wireless units," in *Proc. IEEE Antennas Propag. Int. Symp. 2006*, Albuquerque, NM, pp. 3569–3572.

[3] J. Frolik, T. M. Weller, S. DiStasi, and J. Cooper, "A compact reverberation chamber for hyper-Rayleigh channel emulation," *IEEE Trans. Antennas Propag.*, vol. 57, no. 12, pp. 3962–3968, Dec. 2009.

[4] X. Chen, P.-S. Kildal, C. Orlenius, and J. Carlsson, "Channel sounding of loaded reverberation chamber for over-the-air testing of wireless devices—Coherence bandwidth versus average mode bandwidth and delay spread," *IEEE Antennas Wireless Propag. Lett.*, vol. 8, pp. 678–681, Jun. 2009.

[5] C. Orlenius, P.-S. Kildal, and G. Poilasne, "Measurements of total isotropic sensitivity and average fading sensitivity of CDMA phones in reverberation chamber," in *Proc. IEEE AP-S Int. Symp.*, Washington, DC, Jul. 3–8, 2005, vol. 1A, pp. 409–412.

[6] N. Serafimov, P.-S. Kildal, and T. Bolin, "Comparison between radiation efficiencies of phone antennas and radiated power of mobile phones measured in anechoic chambers and reverberation chambers," in *Proc. IEEE AP-S Int. Symp.*, San Antonio, TX, Jun.2002, vol. 2, pp. 478–481.

[7] C. L. Holloway, D. A. Hill, J. M. Ladbury, P. F. Wilson, G. Koepke, and J. Coder, "On the use of reverberation chambers to simulate a Rician radio environment for the testing of wireless devices," *IEEE Trans. Antennas Propag.*, vol. 54, no. 11, pp. 3167–3177, Nov. 2006.

[8] P.-S. Kildal and K. Rosengren, "Correlation and capacity of MIMO systems and mutual coupling, radiation efficiency, and diversity gain of their antennas: Simulation and measurement in a reverberation chamber," *IEEE Comm. Mag.*, vol. 42, no. 12, pp. 104–112, Dec. 2004.

[9] O. Delangre, P. De Doncker, M. Lienard, and P. Degauque, "Testing MIMO systems with coupled reverberation changers: A wideband channel model," in *Proc. EuCAP 2006*, Nice, France, pp. 1–6.

[10] J. F. Valenzuela-Valdés, A. M. Martínez-González, and D. A. Sánchez-Hernández, "Emulation of MIMO nonisotropic fading environments with reverberation chambers," *IEEE Antennas Wireless Propag. Lett.*, vol. 7, pp. 325–328, 2008.

[11] O. Delangre, S. V. Roy, P. D. Doncker, M. Lienard, and P. Degauque, "Modeling in-vehicle wideband wireless channels using reverberation chamber theory," in *Proc. 66th IEEE Vehic. Technol. Conf.*, Baltimore, MD, Sep. 2007, pp. 2149–2153.

[12] E. Genender, C. L. Holloway, K. A. Remley, J. Ladbury, G. Koepke, and H. Garbe, "Using the reverberation chamber to simulate the power delay profile of a wireless environment," in *Proc. EMC Europe 2008*, Hamburg, Germany, pp. 1–6.

[13] E. Genender, C. L. Holloway, K. A. Remley, J. Ladbury, G. Koepke, and H. Garbe, "Simulating the multipath channel with a reverberation chamber: Application to bit error rate measurements," *IEEE Trans. Electromagn. Compat.*, vol. 52, no. 4, pp. 766–777, Nov. 2010.

[14] O. Delangre, P. De Doncker, F. Horlin, M. Lienard, and P. Degauque, "Reverberation chamber environment for testing communication systems: Applications to OFDM and SC-FDE," in *Proc. 68th IEEE Veh. Technol. Conf.*, Calgary, Canada, Sep. 2008, pp. 1–6.

[15] H. Fielitz, K. A. Remley, C. L. Holloway, D. Matolak, Q. Zhang, and Q. Wu, "Reverberation-chamber test environment for outdoor urban wireless propagation studies," *IEEE Antennas Wireless Propag. Lett.*, vol. 9, pp. 52–56, Feb. 2010.

[16] S. J. Floris, K. A. Remley, and C. L. Holloway, "Bit error rate measurements in reverberation chambers using real-time vector receivers," *IEEE Antennas Wireless Propag. Lett.*, vol. 9, pp. 619–622, Jun. 2010.

[17] T. Rappaport, *Wireless Communications, Principles and Practice*. Upper Saddle River, NJ: Prentice-Hall, 1996.

[18] D. A. Hill, *Electromagnetic Fields in Cavities*. Piscataway, NJ: IEEE Press, 2009.

[19] K. Karlsson, X. Chen, P. S. Kildal, and J. Carlsson, "Doppler spread in reverberation chamber predicted from measurements during step-wise stationary stirring," *IEEE Antennas Wireless Propag. Lett.*, vol. 9, pp. 497–500, May 2010.

[20] M. Matsumoto and T. Nishimura, "Marsenne twister: A 623-dimensionally equidistributed uniform pseudo-random number generator," *ACM TOMACS*, vol. 8, pp. 3–30, Jan. 1998.

[21] W. C. Jakes, Jr., *Microwave Mobile Communications*. New York: Wiley, 1974, ISBN: 0471437204.

[22] P. A. Bello and B. D. Nelin, "The effect of frequency-selective fading on the binary error probabilities of incoherent and differentially-coherent matched filter receivers," *IRE Trans. Commun. Syst.*, vol. COM-11, pp. 170–186, Jun. 1963.

[23] R. J. C. Bultitude, "Estimating Frequency Correlation Functions From Propagation Measurements on Fading Radio Channels: A Critical Review," *IEEE J. Sel. Areas Commun.*, vol. 20, no. 6, pp. 1133–1143, Aug. 2002.

[24] U. Carlberg, P. S. Kildal, A. Wolfgang, and O. Sotoudeh, "Calculated and measured absorption cross sections of lossy objects in reverberation chamber," *IEEE Trans. Electromagn. Compat.*, vol. 46, no. 2, pp. 146–154, May 2004.

[25] M. C. Jeruchim, "Techniques for estimating bit error rate in the simulation of digital communication systems," *IEEE J. Sel. Areas Commun.*, vol. SAC-2, no. 1, pp. 153–170, Jan. 1984.

[26] I. Sen, D. W. Matolak, and W. Xiong, "Wireless channels that exhibit "worse than Rayleigh" fading, *Proc. IEEE MILCOM*, Washington, DC, Oct. 2006, p. 7.

[27] D. W. Matolak and J. Frolik, "Worse-than-Rayleigh fading: Experimental results and theoretical models," *IEEE Commun. Mag.*, to be published.

[28] J. Chuang, "The effects of time delay spread on portable radio communications channels with digital modulation," *IEEE J. Sel. Areas Commun.*, vol. SAC-5, no. 5, pp. 879–889, Jun 1987.

Kate A. Remley (S'92–M'99–SM'06) was born in Ann Arbor, MI. She received the Ph.D. degree in electrical and computer engineering from Oregon State University, Corvallis, OR, in 1999.

From 1983 to 1992, she was a Broadcast Engineer in Eugene, OR, and from 1989 to 1991, she was a Chief Engineer of an AM/FM broadcast station. In 1999, she joined the Electromagnetics Division, National Institute of Standards and Technology, Boulder, CO, as an Electronics Engineer. Her current research interests include metrology for wireless systems, characterizing the link between nonlinear circuits and system performance, and developing methods for improved radio communications for the public-safety community.

Dr. Remley was the recipient of the Department of Commerce Bronze and Silver Medals and an Automatic RF Techniques Group Best Paper Award. She is currently the Editor-in-Chief of IEEE Microwave Magazine and an Immediate Past Chair of the MTT-11 Technical Committee on microwave measurements.

Sander J. Floris was born in 1984 in Drachten, The Netherlands. He received the B.Sc. degree in electrical engineering from Eindhoven University of Technology, Eindhoven, The Netherlands, in 2007, where he is currently working toward the Ph.D. degree in the Electromagnetics Group, Department of Electrical Engineering.

In 2008, he was a Guest Researcher at the Electromagnetics Division, National Institute of Standards and Technology, Boulder, CO. His current research interests include numerical and physical aspects of electromagnetic fields.

Haider A. Shah was born in Peshawar, Pakistan, in 1985. He received the B.S. degree in electrical engineering from COMSATS Institute of Information Technology, Islamabad, Pakistan, in 2007, and the M.S. degree in communication engineering from Chalmers University of Technology, Gothenburg, Sweden, in 2010.

From June 2007 to July 2008, he was with Nokia Siemens Networks as a Base Station Subsystem Engineer. In 2010, he was a Guest Researcher at the National Institute of Standards and Technology, Boulder, CO. He is currently a radio-system integration engineer at Ericsson, Stockholm, Sweden. His current research interests include wireless communications and signal processing.

Christopher L. Holloway (S'86–M'92–SM'04–F'10) received the B.S. degree from the University of Tennessee, Chattanooga, in 1986, and the M.S. and Ph.D. degrees from the University of Colorado, Boulder in 1988 and 1992, respectively, both in electrical engineering.

In 1992, he was a Research Scientist with Electro Magnetic Applications, Inc., Lakewood, CO, where he was engaged with theoretical analysis and finite-difference time-domain modeling of various electromagnetic problems. From the fall of 1992 to 1994, he was with the National Center for Atmospheric Research, Boulder, CO, where he was involved with wave propagation modeling, signal processing studies, and radar systems design. From 1994 to 2000, he was with the Institute for Telecommunication Sciences, U.S. Department of Commerce, Boulder, where he was involved in wave propagation studies. Since 2000, he has been with the National Institute of Standards and Technology, Boulder, where he works on electromagnetic theory. He is also on the Graduate Faculty at the University of Colorado, Boulder. His current research interests include electromagnetic field theory, wave propagation, guided wave structures, remote sensing, numerical methods, and electromagnetic compatibility (EMC)/electromagnetic interference issues.

Dr. Holloway is currently a Co-Chair for Commission A of the International Union of Radio Science. He is also an Associate Editor for the IEEE TRANSACTIONS ON ELECTROMAGNETIC COMPATIBILITY. From 2000 to 2005, he was the Chairman for the Technical Committee on Computational Electromagnetics (TC-9) of the IEEE Electromagnetic Compatibility Society. From 2004 to 2006, he was an IEEE Distinguished Lecturer for the EMC Society. He is also a Co-Chair for the Technical Committee on Nanotechnology and Advanced Materials (TC-11) of the IEEE EMC Society.